Video Article

DNA Nanotubes as a Versatile Tool to Study Semiflexible Polymers

Jörg Schnauß*[1,2], Martin Glaser*[1,2], Jessica S. Lorenz[1], Carsten Schuldt[1,2], Christin Möser[1], Martin Sajfutdinow[1], Tina Händler[1,2], Josef A. Käs[2], David M. Smith[1]

[1]Fraunhofer Institute for Cell Therapy and Immunology

[2]Institute of Experimental Physics I, Universität Leipzig

*These authors contributed equally

Correspondence to: Jörg Schnauß at joerg.schnauss@izi.fraunhofer.de, David M. Smith at david.smith@izi.fraunhofer.de

URL: https://www.jove.com/video/56056
DOI: doi:10.3791/56056

Keywords: Bioengineering, Issue 128, Rheology, semiflexible polymers, persistence length, DNA tubes, biopolymers, actin, hydrogel, networks

Date Published: 10/25/2017

Citation: Schnauß, J., Glaser, M., Lorenz, J.S., Schuldt, C., Möser, C., Sajfutdinow, M., Händler, T., Käs, J.A., Smith, D.M. DNA Nanotubes as a Versatile Tool to Study Semiflexible Polymers. *J. Vis. Exp.* (128), e56056, doi:10.3791/56056 (2017).

Abstract

Mechanical properties of complex, polymer-based soft matter, such as cells or biopolymer networks, can be understood in neither the classical frame of flexible polymers nor of rigid rods. Underlying filaments remain outstretched due to their non-vanishing backbone stiffness, which is quantified via the persistence length (l_p), but they are also subject to strong thermal fluctuations. Their finite bending stiffness leads to unique, non-trivial collective mechanics of bulk networks, enabling the formation of stable scaffolds at low volume fractions while providing large mesh sizes. This underlying principle is prevalent in nature (*e.g.,* in cells or tissues), minimizing the high molecular content and thereby facilitating diffusive or active transport. Due to their biological implications and potential technological applications in biocompatible hydrogels, semiflexible polymers have been subject to considerable study. However, comprehensible investigations remained challenging since they relied on natural polymers, such as actin filaments, which are not freely tunable. Despite these limitations and due to the lack of synthetic, mechanically tunable, and semiflexible polymers, actin filaments were established as the common model system. A major limitation is that the central quantity l_p cannot be freely tuned to study its impact on macroscopic bulk structures. This limitation was resolved by employing structurally programmable DNA nanotubes, enabling controlled alteration of the filament stiffness. They are formed through tile-based designs, where a discrete set of partially complementary strands hybridize in a ring structure with a discrete circumference. These rings feature sticky ends, enabling the effective polymerization into filaments several microns in length, and display similar polymerization kinetics as natural biopolymers. Due to their programmable mechanics, these tubes are versatile, novel tools to study the impact of l_p on the single-molecule as well as the bulk scale. In contrast to actin filaments, they remain stable over weeks, without notable degeneration, and their handling is comparably straightforward.

Video Link

The video component of this article can be found at https://www.jove.com/video/56056/

Introduction

Due to the complex behaviors enabled by their unique mechanical properties, semiflexible polymers are fundamental building blocks of living matter. In contrast to flexible polymers, semiflexible polymers adopt an outstretched configuration due to their non-vanishing backbone stiffness while still remaining subject to strong thermal fluctuations[1]. Thus, purely stochastic models cannot be applied to their behaviors, as with the extremes of fully flexible or rigid polymers. The so-called worm-like chain model[2,3,4] was developed to quantify this stiffness via the l_p, which is the decay constant of the tangent-tangent correlation along the filament[4]. If l_p is comparable to the contour length (l_c) of the filament, the polymer is considered semiflexible[1]. Analogous to the poles of a tent, their arrangements in networks or bundles stabilizes the entire collective system at low volume fractions, leading to unusual viscoelastic properties[5,6,7,8,9]. These structures provide high elasticities at large mesh sizes[10], maintaining mechanical integrity while still facilitating diffusive and active transport processes. This property is especially suitable for biological systems such as the cytoskeleton or the extracellular matrix, but it is also widely used in food engineering[1,11,12].

Going beyond their significance to living matter, it is crucial to comprehensively examine the physical properties of these structures in order to have the tools to develop biomimetic materials or novel hydrogels. In terms of semiflexible polymers, this implies the systematic determination of the collective properties of networks resulting from single-filament properties such as l_p and the development of a descriptive theoretical framework. In pioneering studies, the cellular biopolymer actin was established as a model system for semiflexible polymers and is still widely considered the gold standard[5,13,14,15,16,17]. However, exhaustive studies are limited with this system since they are bound to the inherent properties of this protein. Various theoretical approaches have aimed at building a description of the non-trivial mechanical behaviors at the single-filament level and have led to notably different scaling predictions for the dependence of the linear elastic plateau shear modulus, G_0 (*i.e.,* the "elasticity" of the network), with respect to concentration (c) and l_p[6,7,13,14,15,18,19,20,21,22,23]. While the concentration scaling is readily accessible in experiments with actin-based or other model systems and while theoretical predictions have been rigorously verified[13,16,24,25], the scaling with respect to l_p has remained experimentally inaccessible. This, however, is a major limitation since l_p is also an independent variable that is the defining quantity of semiflexible polymers.

This central, natural limitation imposed by the fixed l_p of actin or other biologically-derived polymers such as collagen has recently been resolved by employing tile-based DNA tubes, which are tunable in their mechanical properties[9,26,27,28]. Slight variations in the architectures of the tubes (*e.g.,* different numbers of constituent DNA strands within the unit ring) yield distinct values for l_p, which can be evaluated via fluorescence microscopy, either by analyzing one fluctuating tube or by evaluating the curved configurations of several adhered tubes, as described previously[9,28]. These analyses revealed that l_p values of the different tube populations vary over more than one order of magnitude and that different evaluation techniques yield consistent results[9,28].

Surprisingly, the overall scaling of the linear elastic plateau shear modulus G_0 with respect to the concentration and l_p has been reported to be inconsistent with all previous theoretical approaches[9], in particular demonstrating a much stronger than predicted dependence upon l_p. These findings emphasize the value of a new model system to study the central properties of semiflexible polymers. Employing *n*-helix DNA tubes dramatically broadens the scope of these investigations. Not only can l_p be freely varied without changing the basic material, but the inherent programmable nature of DNA can enable the systematic examination of additional elements, such as crosslinks or kinetic switching processes. Additionally, these tubes are soluble in water and, in contrast to most proteins, stable in adequate pH and ionic conditions for several weeks, without detectable degradation[9].

To assemble these tubes, a discrete set of DNA oligonucleotides is used, each of which contains two domains that share complementary base sequences to two neighboring strands (due to the specific sequences, a single strand cannot form structures such as hair pins). The complementary sequences hybridize in a cyclic manner, forming enclosed, half-overlapping rings of *n* interconnected double-helical segments (**Figure 1A** and **B**). These rings form at a discrete diameter (**Figure 1C**), and their half-overlapping configuration exposes axial sticky ends complementary to the sticky ends of another ring. This selective addition of matching oligonucleotides triggers a stacking of the rings, leading to the effective polymerization of filamentous DNA helix tubes of size *n* (*n*HT). Their contour lengths typically measure several microns in length, and their length distribution is comparable to that of actin filaments[9,26,27,28]. It has been shown for similar DNA nanotubes that they indeed exhibit polymerization kinetics similar to those of actin filaments and microtubules[29]. Depending on the number *n* of individual DNA strands making up the basic ring structure, the *n*HT architecture, as well as its circumference and diameter, can be controllably varied. Using more DNA strands increases the circumference of the rings/tubes, and the corresponding architectural change shifts the mechanical properties to higher l_p values (**Figure 1C**), corresponding to a higher rigidity. On the mesoscopic scale, these larger l_p values translate into less bent conformations due to the higher stiffness (**Figure 1D** and **E**).

Protocol

1. Preparation of *n* HTs

NOTE: Here, *n* denotes the number of different single DNA strands involved in the formation of the helix tubes of a certain size. For *n*=8, eight different single DNA strands make up a unit ring.

1. Purchase DNA sequences (HPLC purity grade or higher) from a suitable DNA synthesis service or perform high-quality synthesis and purification (exemplary sequences given in **Table 1**).
2. Resuspend lyophilized oligonucleotides in purified water and follow the further resuspension steps given in the corresponding manual from the company. Adjust the amount of water to obtain a final concentration of 200 µM.
3. Determine concentrations of the single DNA strands to verify the values given by the distributor (*e.g.,* via UV-Vis spectroscopy at 260 nm) since the exact stoichiometry is crucial for the assembly process. Calculate the concentration of the oligonucleotides, taking into account the specific molar weight and the extinction coefficient for each single-stranded DNA oligonucleotide.
   NOTE: The extinction coefficient values inherently vary for the different sequences and are stated in the documentation of commercially purchased DNA. They can also be calculated according to the nearest-neighbor model using a number of freely available online tools. To comply with the linear range of the spectrometer, consider diluting the sample used for concentration determination.
4. Using a micropipette, mix the DNA strands-each at the same concentration-in a container suitable for the thermocycler (*e.g.,* a 200 µL PCR tube) to form the desired *n*HTs (final buffer conditions: 1xTE (10 mM Tris and 1 mM EDTA, pH 8) and 12.5 mM $MgCl_2$).
   NOTE: Final DNA *n*HT samples consist of *n*- 1 strands, U_1− U_{n-1}, and one T*n* strand. The concentration per strand can vary from sub-micromolar to more than 10 µM, depending on the needs of the user (*e.g.,* <1 µm per strand for the subsequent dilution to observe single filaments or higher concentrations for the examination of dense network mechanics).
5. Hybridize the *n*HTs in a thermocycler (denaturation for 10 min at 90 °C, with a subsequent quick drop to 65 °C; slow temperature decrease from 65 °C to 55 °C, with complementary base pairing in 20 temperature steps of -0.5 K for 30 min each; and a quick drop from 55 °C to 20 °C); see **Figure 2A**.
   NOTE: The slow decrease steps from 65 °C can be lengthened to increase the average tube length; however, the subsequent quick drop to 20 °C is crucial to avoid the aggregation of polymerized tubes.
6. Store the hybridized *n*HTs for up to 3 weeks at 4 °C without detectable degradation.
   NOTE: For fluorescence microscopy, labeled *n*HTs are hybridized by (partly) substituting U1 with the modified U1-Cy3 (**Table 1**). For longer observation times, the addition of established anti-bleaching agents is advisable.
7. Carefully dilute the sample to the desired final concentration (*e.g.,* 4 µM for networks or 20 nM for single-filament observations) using the sample buffer, if necessary. To minimize possible error sources, assemble samples at the desired final concentration.

2. Shear Rheology

1. Choose an appropriate geometry (plate-plate or cone-plate) for the dynamic shear rheometer. For small volumes (*i.e.,* below 200 µL), use the cone-plate geometry.
2. Load the sample on the dynamic shear rheometer.
3. **Passivate the air-water interface of the sample and environment using the following steps to prevent potential evaporation effects.**
   1. Surround the sample with 2.5 mL of the sample buffer bath.

2. Add a surfactant just below the micelle concentration.
3. Use a Hamilton syringe to surround the sample with a lipid to avoid direct contact of the sample with air.

4. Seal the sample chamber with a cap equipped with wet sponges and, if possible, with an additional water bath (not in contact with the sample) to further suppress evaporation.
5. Start the measurement using the rheometer-specific software at room temperature; alternatively, perform the measurement at different temperatures, such as 37 °C (if physiological conditions are needed).
   NOTE: Cooling the sample is often accompanied by the condensation of water vapor from the surrounding air, while heating leads to enhanced evaporation. Both effects can uncontrollably change the concentration of the sample, so all measurements in a series should be performed at a constant temperature.
6. Allow the sample to equilibrate for 2 h at room temperature. The time evolution may be monitored with a time sweep (one data point per minute; strain γ = 5%; frequency f = 1 Hz).
7. **Measure the mechanical properties with the desired test protocols. Start with a series of frequency sweeps (*f*-sweeps) because they leave the sample intact and allow for more measurements.**
   NOTE: Additionally, short *f*-sweeps should be carried out before and after longer measurements (such as long *f*-sweeps with a much higher resolution) to verify that the sample remained unchanged throughout the full measurement protocol.
   1. Perform a short *f*-sweep (*e.g.,* γ = 5%; f = 0.01 Hz to 30 Hz; 5 data points per decade).
   2. Perform a long *f*-sweep (*e.g.,* γ = 5%; f = 0.001 Hz to 30 Hz; 21 data points per decade); the low-frequency regime can be omitted if not necessary to reduce measurement time.
   3. Perform a short *f*-sweep.
   4. Perform a γ-sweep (*e.g.,* f = 1 Hz; γ = 0.0125% to 100%; 20 data points per decade).
      NOTE: Use the short *f*-sweep first, as it is usually inconsistent with previous *f*-sweeps because networks usually rupture during γ-sweep or detach from the plates. Alternatively, use γ-ramp (*e.g.,* = 0.025 s^{-1}, t = 60 s); however, the ramps usually require changing the motor mode, so subsequent short *f*-sweeps would be falsified.

8. Bin and/or smooth the raw data with a Gaussian kernel.

3. Fluorescence-assisted Analysis of DNA Annealing

1. Prepare 8 aliquots of 12 µL for each sample using 1-4 µM DNA per strand, 12.5 mM $MgCl_2$ in 1x TE buffer, and 1x nucleic acid gel stain from a 10,000x DMSO stock. Make a negative control with no DNA, but include nucleic acid gel stain.
2. Transfer the aliquots to a real-time PCR plate and seal with adhesive film (*e.g.,* a 96-well reaction plate).
   NOTE: The high temperatures used in the thermal annealing protocols will evaporate samples. Thus, make sure that the wells are tightly sealed with adhesive film to prevent water evaporation and concentration increase, particularly during long-term experiments.
3. Centrifuge the plate at 100 x g for 1 min at room temperature to remove the gas bubbles; if the gas bubbles expand, the wells cannot be analyzed.
4. Load the sealed plate into a real-time quantitative PCR system.
5. Run an annealing program. Denature the DNA at 90 °C for 10 min. Drop the temperature quickly to 72 °C. Then, decrease the temperature slowly by 0.5 °C every 30 min. After the signal has decayed, accelerate the temperature ramp.
   NOTE: 72 °C is sufficiently above the real hybridization temperature; thus, the signal is recorded over a broad temperature range suitable for determining the necessary temperature range.
6. Make sure that the lid of the cycler heats to at least 100 °C to prevent the condensation of evaporated sample on the adhesive film.
7. During assembly, excite the samples with an argon-ion laser at 488 nm and detect the fluorescence at 550 nm when using a nucleic acid gel stain (or spectrally similar). For other dyes, choose an appropriate excitation/emission combination. Measure the fluorescence signal as often as possible to increase the overall signal quality using the built-in camera.
   NOTE: Here, measurements were taken every 9 s.
8. If preset melting and annealing programs are applied, use the provided software to analyze the data. If not, subtract the previous mean value from the mean value for each temperature step to obtain the relative change of the fluorescent signal.

4. AFM Imaging

1. Cleave mica (*e.g.,* mica "V1") by attaching commercially available adhesive tape and ripping it off; the uppermost layer of the mica should be removed.
2. Using a micropipette, deposit pre-formed *n*HT in Mg^{2+} containing folding buffer on the freshly cleaved mica and let it settle for 10 min.
3. Spin the samples in short 3-s intervals at 2,000 x g on a small table centrifuge to remove the remaining liquid. Several *n*HTs should still be attached to the mica surface.
4. Use a cantilever tip with a high stiffness (*e.g.,* 54 Nm^{-1}) and determine its resonance frequency with the internal AFM software.
5. Record the height profile with the AFM in air in tapping mode at low scan rates (*e.g.,* 1 line/s) to avoid damaging or displacing the *n*HTs.

Representative Results

The assembly of DNA nanotubes via a temperature ramp (**Figure 2**) is a very reliable method to form these artificial semiflexible polymers. These polymers have comparable characteristics to their naturally occurring counterparts, such as actin filaments, but provide a much broader experimental framework since their mechanical properties can be controllably altered[9,27]. Like biopolymers, they can be arranged in networks (**Figure 3**) and specifically allow one to test the impact of the filament stiffness on bulk structures and properties. As shown in **Figure 4**, these networks display a linear strain regime for strains up to 10%, which closely resembles the characteristics of networks of actin filaments. Within this regime, linear shear rheology can be readily applied, for instance, to determine the elastic and viscous response of DNA nanotube networks probed at different frequencies[9]. These tests reveal that those networks predominantly behave elastically (**Figure 5**). In contrast to measurements with proteins, these tubes do not denature at the air-water interface of the sample and therefore, sophisticated passivation strategies are required (**Figure 6**). Therefore, the handling of the samples is rather straightforward and has proven to be very robust, yielding consistent results with low sample-to-sample variations.

However, the question of whether the free "sticky ends" of unpaired single-stranded DNA at both ends of each tube can induce undesired, stochastic hybridization events remained. To address this concern, complementary "end cap" sequences covering the ends of the tube were added to the sample after the hybridization process was complete. However, **Figure 7** illustrates that capping the ends of the filaments has no detectable influence and that the tube ends do not induce any transient crosslinking effect in the network[9]. Sticking events only play a significant role when the sample is handled too roughly and the tubes break due to harsh pipetting. These breakage points indeed appear to induce crosslinking effects, leading to non-linear responses of the system, such as strain stiffening (**Figure 8**).

If the samples are carefully prepared, they can be used to test the impact that either the filament concentration (**Figure 9A**) or the filament stiffness (**Figure 9B**)[9] have on the mechanical properties of networks consisting of semiflexible polymers. For the first time, the quantitative connection between the filament stiffness and network elasticity was studied experimentally and systematically, yielding a linear power law behavior, which contradicts predominant theoretical predictions. These results illustrate that DNA nanotubes are a new, versatile tool to study the effects of semiflexible polymers, which were formerly experimentally inaccessible[9,27]. Now, various theories can be experimentally tested, involving statements about dependencies on the persistence length l_p of the filaments. Additionally, very fundamental effects, such as reptation (**Figure 10**), can be investigated from various perspectives by employing tubes that vary in stiffness.

Name	Sequence
U1: a1*-b1*-a2-b2	GGCGATTAGG-ACGCTAAGCCA-CCTTTAGATCC-TGTATCTGGT
U1-Cy3: a1*-b1*-a2-b2	Cy3-TTGGCGATTAGG-ACGCTAAGCCA-CCTTTAGATCC-TGTATCTGGT
U2: a2*-b2*-a3-b3	GGATCTAAAGG-ACCAGATACA-CCACTCTTCC-TGACATCTTGT
U3: a3*-b3*-a4-b4	GGAAGAGTGG-ACAAGATGTCA-CCGTGAGAACC-TGCAATGCGT
U4: a4*-b4*-a5-b5	GGTTCTCACGG-ACGCATTGCA-CCGCACGACC-TGTTCGACAGT
U5: a5*-b5*-a6-b6	GGTCGTGCGG-ACTGTCGAACA-CCAACGATGCC-TGATAGAAGT
U6: a6*-b6*-a7-b7	GGCATCGTTGG-ACTTCTATCA-ATGCACCTCC-AGCTTTGAATG
U7: a7*-b7*-a8-b8	GGAGGTGCAT-CATTCAAAGCT-AACGGTAACTA-TGACTTGGGA
U8: a8*-b8*-a9-b9	TAGTTACCGTT-TCCCAAGTCA-AACACTAGAC-ACATGCTCCTA
U9: a9*-b9*-a10-b10	GTCTAGTGTT-TAGGAGCATGT-CGAGACTACAC-CCTTGCCACC
U10: a10*-b10*-a11-b11	TGTAGTCTCGG-GTGGCAAGGG-TACTACCGCT-CCATTAAGAAT
U11: a11*-b11*-a12-b12	AGCGGTAGTA-ATTCTTAATGG-ATCCGTCTATC-TACACTATCA
U12: a12*-b12*-a13-b13	ATAGACGGATT-GATAGTGTAG-AGACGAAATC-AGCAGAACTAA
U13: a13*-b13*-a14-b14	GATTTCGTCT-TTAGTTCTGCT-CTGCGAAGTAA-TCAGCCGAGC
T4: a4*-b4*-a1-b1	GGTTCTCACGG-ACGCATTGCA-CCTAATCGCC-TGGCTTAGCGT
T5: a5*-b5*-a1-b1	GGTCGTGCGG-ACTGTCGAACA-CCTAATCGCC-TGGCTTAGCGT
T6: a6*-b6*-a1-b1	GGCATCGTTGG-ACTTCTATCA-CCTAATCGCC-TGGCTTAGCGT
T7: a7*-b7*-a1-b1	GGAGGTGCAT-CATTCAAAGCT-CCTAATCGCC-TGGCTTAGCGT
T8: a8*-b8*-a1-b1	TAGTTACCGTT-TCCCAAGTCA-CCTAATCGCC-TGGCTTAGCGT
T9: a8*-b8*-a1-b1	GTCTAGTGTT-TAGGAGCATGT-CCTAATCGCC-TGGCTTAGCGT
T10: a10*-b10*-a1-b1	GTGTAGTCTCG-GGTGGCAAGG-CCTAATCGCC-TGGCTTAGCGT
T14: a14*-b14*-a1-b1	TTACTTCGCAG-GCTCGGCTGA-CCTAATCGCC-TGGCTTAGCGT
end cap A1	CCTAATCGCC
end cap A2	CCTTTAGATCC
end cap A3	CCACTCTTCC
end cap A4	CCGTGAGAACC
end cap A5	CCGCACGACC
end cap A6	CCAACGATGCC
end cap A7	ATGCACCTCC
end cap A8	AACGGTAACTA
end cap B1*	ACGCTAAGCCA
end cap B2*	ACCAGATACA
end cap B3*	ACAAGATGTCA
end cap B4*	ACGCATTGCA
end cap B5*	ACTGTCGAACA
end cap B6*	ACTTCTATCA
end cap B7*	CATTCAAAGCT
end cap B8*	TCCCAAGTCA

Table 1: Example of DNA sequences for the hybridization of the *n*HTs displayed in Figure 1C, which were also used in previous studies on *n*HTs[9,26,27,28]. The given set of sequences allows for the assembly of seven different tube architectures (*e.g.,* a1 hybridizes with the complementary sequence a1*). Other tube architectures not given here can also be formed by the addition or subtraction of strands accompanied by the according cyclization of strand *n* with U_1.

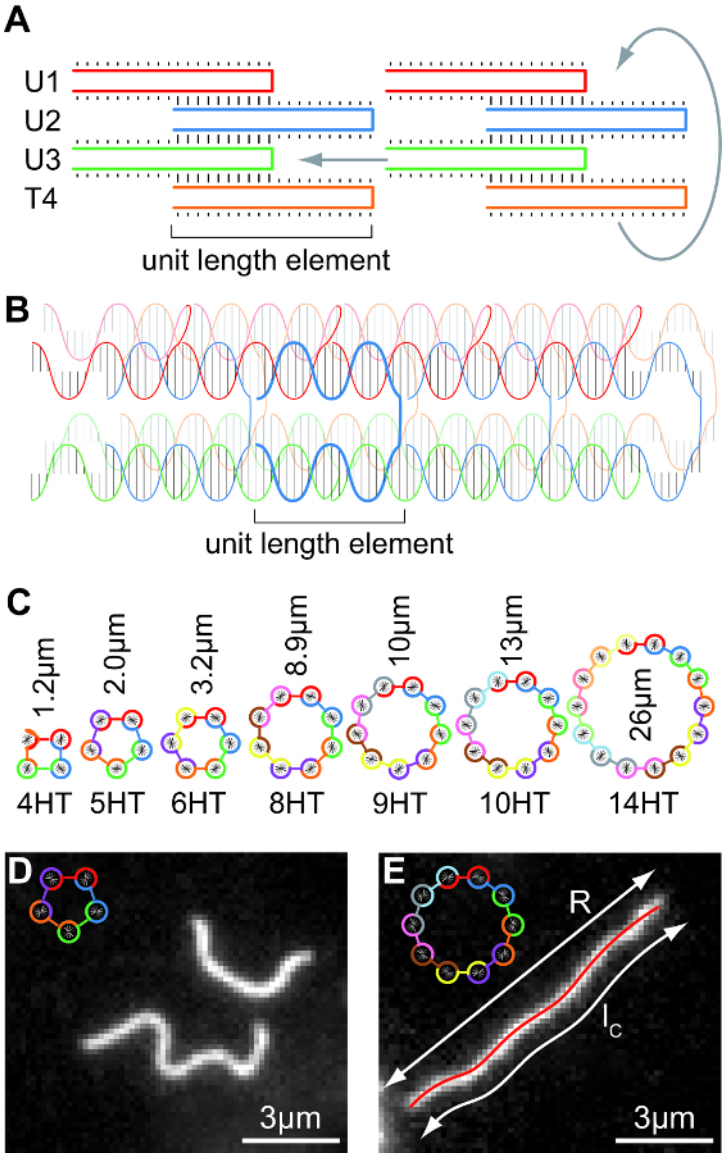

Figure 1: Tube assembly and architecture. (A) Schematic of the assembly of a 4HT formed of four distinct 42-mers. Adjacent single-stranded DNA strands hybridize through continuous alternating domains of 10-11 bases, indicated by long black ticks (the short black ticks indicate unhybridized bases). This half-staggered motif features sticky ends on both sides along the axis, enabling axial growth, indicated by the arrow. The boundary strands U1 and T4 also feature complementary domains and thus form a closed ring, as indicated by the right arrow. Note that this sketch is a 2D representation; in the hybridized state, the strands form double helices and all bases are paired. **(B)** Quasi-3D schematic of a 4HT tetramer with two double helices covered in the shaded distant layer. Double helices form for complementary domains and are linked to both adjacent double helices of the tube once per unit length element. One U2 strand is drawn thicker for clarity. **(C)** Examples of seven different tube architectures are given, with strand numbers ranging from 4 HT to 14 HT and l_p ranging from 1.2 to 26 µm. **(D** and **E)** Epi-fluorescent images of Cy3-labeled, adsorbed 5 HT and 10 HT illustrate the different stiffnesses via differently curved contours. The red overlay is the filament contour found via image analysis, with end-to-end distance R and contour length l_C. Figure adapted from Schuldt *et al*[9]. Please click here to view a larger version of this figure.

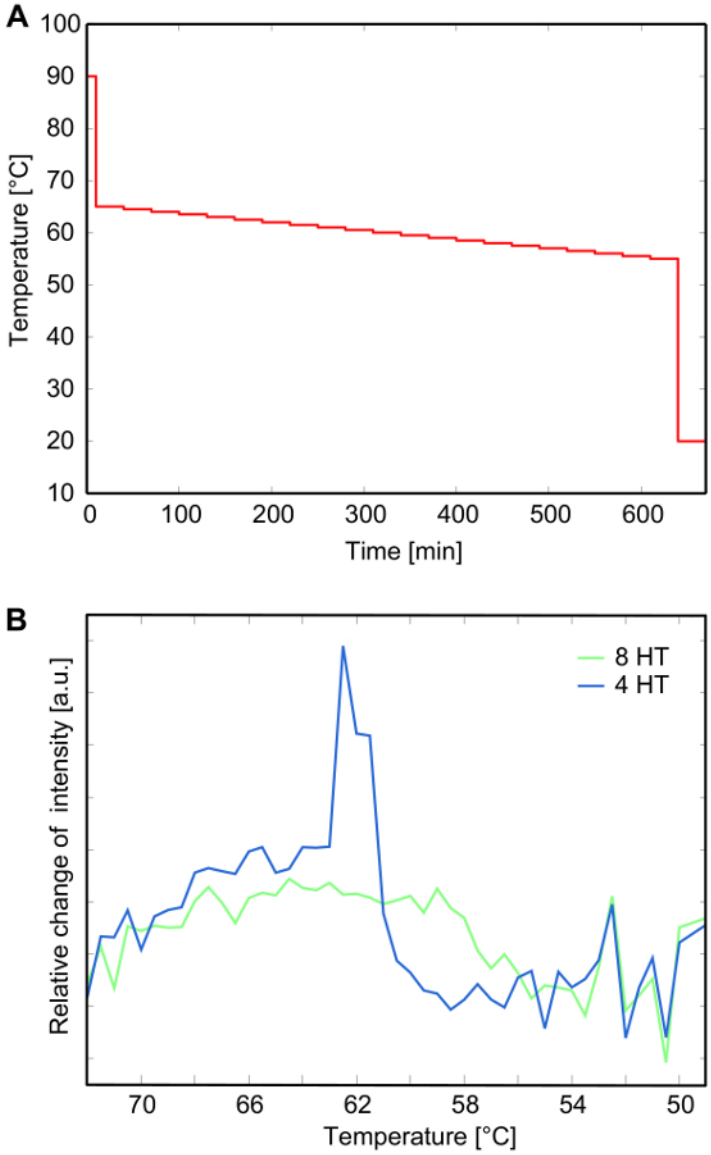

Figure 2: Temperature ramp and corresponding assembly of DNA nanotubes. (A) DNA nanotubes are assembled in a thermocycler via a protocol containing several distinct temperature steps over roughly 11 h. **(B)** In a real-time quantitative PCR system, the relative change of the fluorescent signal of stained strands is a measure for newly formed double-stranded DNA while going through the temperature ramp. Depending on the type of DNA nanotubes, the assembly rate can differ. The more complex the forming structure, the broader the assembly, presumably since more strands (and therefore more segments with distinct sequences and local annealing temperatures) need to hybridize at the appropriate positions, a process which is driven by stochastic thermal fluctuations. Please click here to view a larger version of this figure.

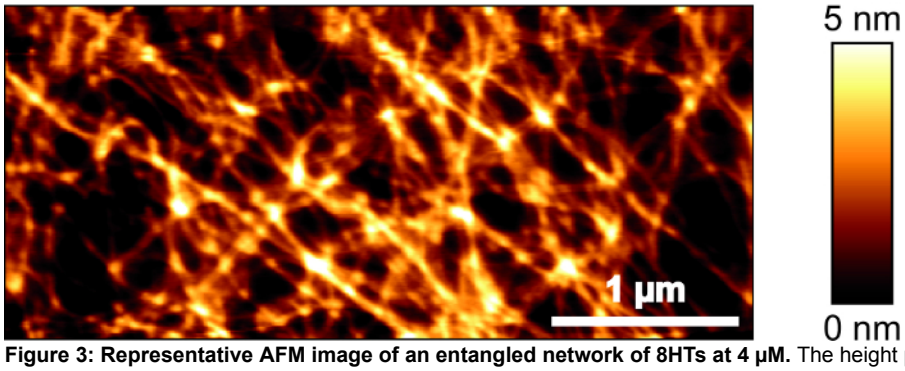

Figure 3: Representative AFM image of an entangled network of 8HTs at 4 µM. The height profile of a preformed network of 8HTs absorbed to a mica surface was recorded using tapping mode in air. AFM images visualize a 2D projection of the network but do not allow for the reliable extraction of data (*e.g.,* mesh size) for the 3D case since the tubes as well as the networks are compressed in a 2D configuration. Please click here to view a larger version of this figure.

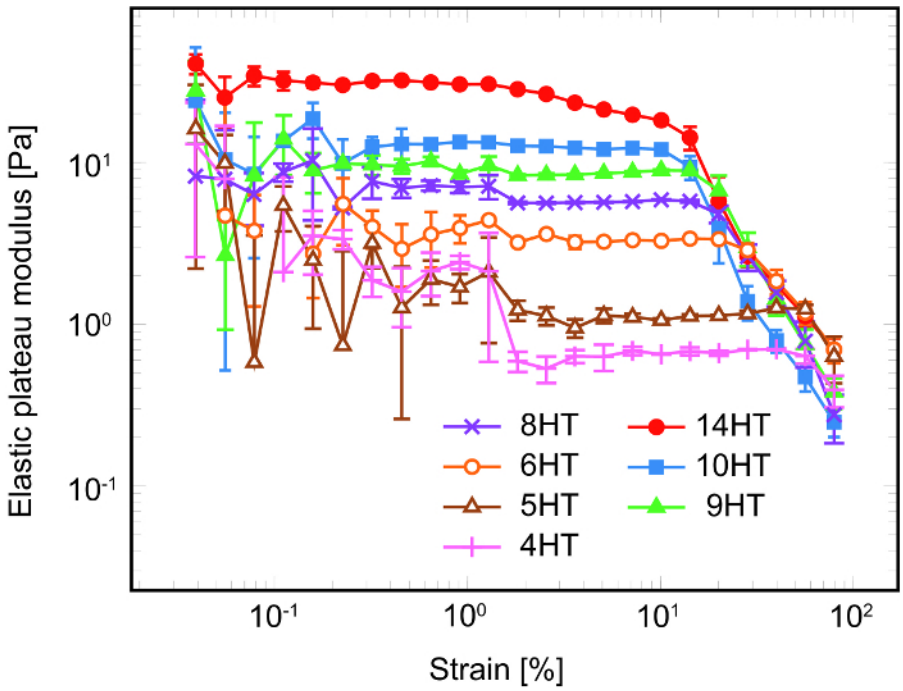

Figure 4: Linear range. Strain measurements (*G*' = 1 Hz) reveal a broad linear elastic plateau, without signs of crosslinking effects such as the non-linear behavior manifesting as strain hardening. Above a characteristic strain (different for each *n*HT), the elastic plateau modulus breaks off irreversibly. The error bars each represent the standard deviation of the mean value of all performed measurements. Figure adapted from Schuldt *et al*[9]. Please click here to view a larger version of this figure.

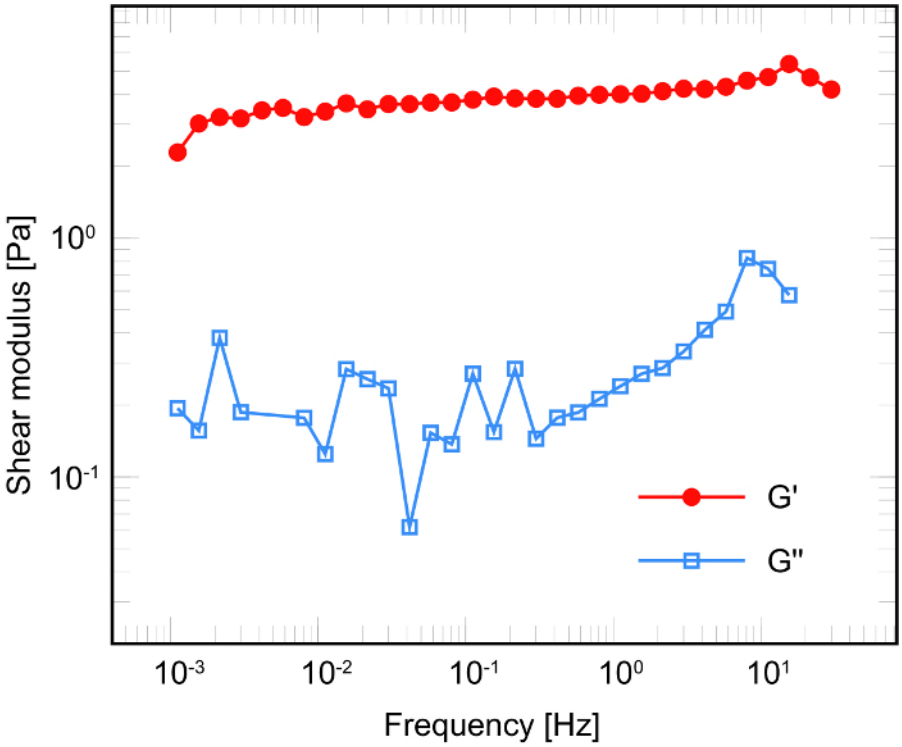

Figure 5: Typical frequency dependence of an entangled 6HT network. Networks of DNA tubes show a broad elasticity plateau over four orders of magnitude, depending on the applied frequency. As expected for a polymer network, the elastic part (*G*') of the complex shear modulus is significantly higher than the viscous part (*G*"). Figure adapted from Schuldt *et al*[9]. Please click here to view a larger version of this figure.

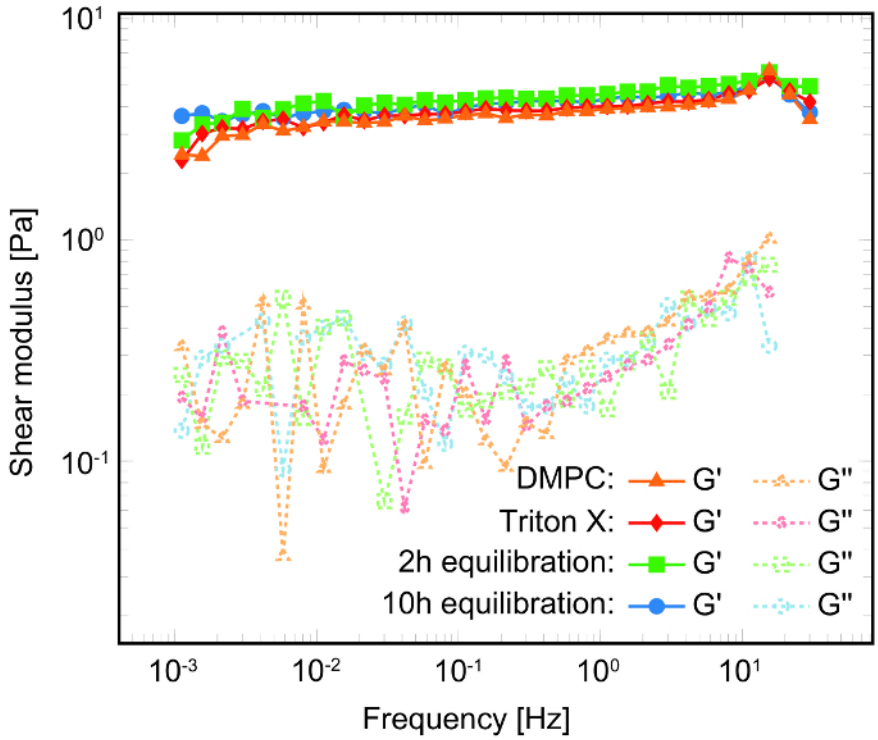

Figure 6: No air-liquid interface effects. Frequency sweeps (*f*-sweeps; γ = 5%) of 8HT samples at 8 µM revealed that the influence of evaporation and gelation effects at the air-water interface are negligible. Different equilibration times, as well as two methods known to drastically reduce protein clustering at the interface (surfactants and lipids), were used. Independent of the method, no indication of drastic influences by evaporation or surface elasticity were recorded. Here, G' represents the elastic modulus and G" represents the viscous modulus (dashed lines). Figure adapted from Schuldt *et al*[9]. Please click here to view a larger version of this figure.

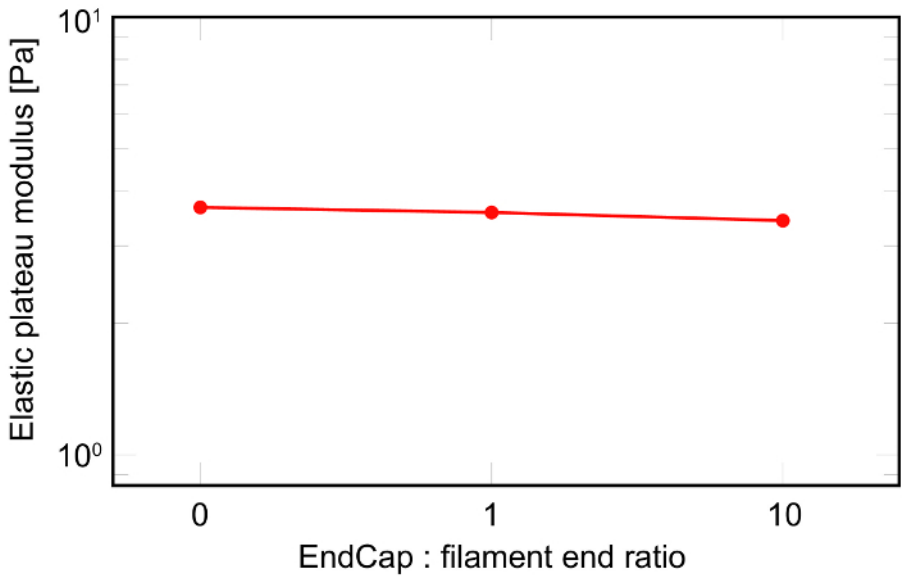

Figure 7: No influence of end modification. The elastic plateau modulus remains constant when capping the sticky free ends of the 8HTs with their respective complementary sequences. Figure adapted from Schuldt *et al*[9]. Please click here to view a larger version of this figure.

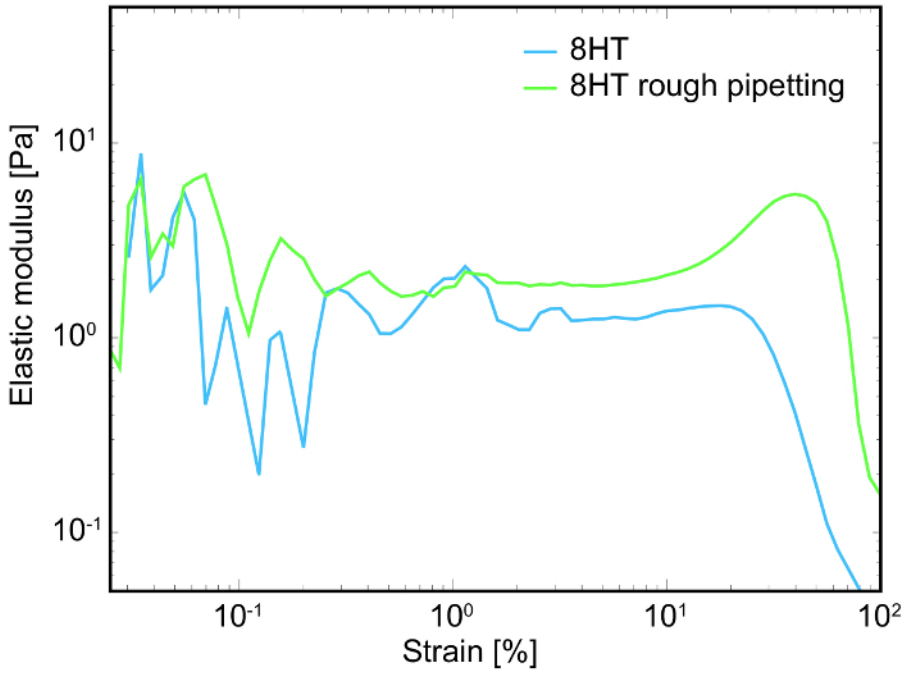

Figure 8: Influence of the handling procedures of the preformed DNA networks on the measurement. Depending on how the preformed networks are handled after hybridization, the measurements may differ. In this example, the shear flow during pipetting of the DNA nanotubes has been drastically varied, and tubes broke if handled too roughly. Breakage leads to unwanted interactions between exposed, complementary single-strands correlating to broken or ruptured segments, which leads to an increase in the elasticity and induces non-linear effects, such as strain hardening (increase of elasticity for large strains, green curve). Please click here to view a larger version of this figure.

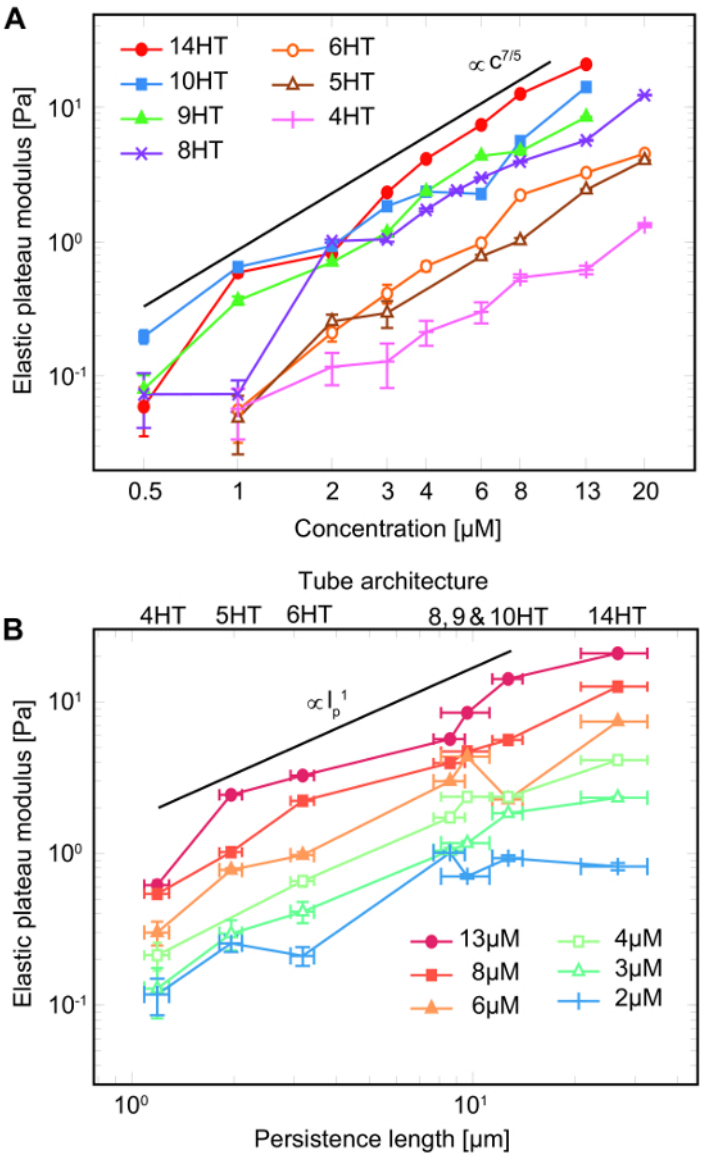

Figure 9: DNA nanotubes enable the study of l_p dependencies. (A) Studying networks of semiflexible polymers with *n*HTs enables the investigation of the mechanical response of the system with increasing concentration (concentration sweep), analogous to studies based on biopolymers such as actin. **(B)** Additionally, the different architectures of the tubes facilitate the determination of the mechanical response with respect to the varying l_p of the underlying filaments, which is infeasible with naturally occurring semiflexible polymers. For this purpose, the data from **A** is replotted to address the scaling of the elastic plateau modulus with respect to l_p. The error bars each represent the standard deviation of the mean value of all performed measurements. Figure adapted from Schuldt *et al*[9]. Please click here to view a larger version of this figure.

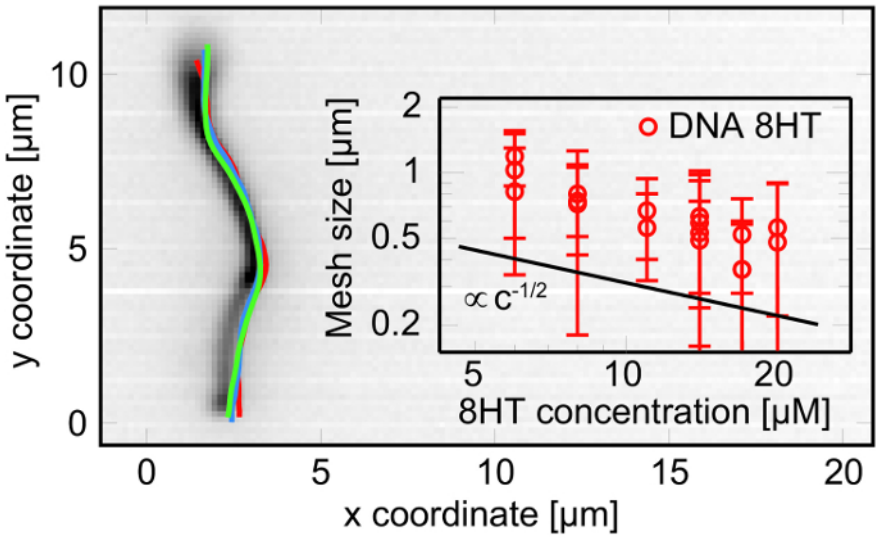

Figure 10: Reptation and mesh size. Recording fluorescence images of reptating filaments (single-labeled DNA 8HT embedded in an unlabeled network; c = 14 µM) can be used to verify the entangled nature of the filaments in the network. Any crosslinking effects would impede this one-dimensional diffusion. Inset: Reptation analysis can be used to determine the mesh size scaling with concentrations, which compares well to actin measurements and agrees with theoretical predictions[30]. The error bars each represent the standard deviation of the mean value of all performed measurements. Figure adapted from Schuldt *et al*[9]. Please click here to view a larger version of this figure.

Discussion

To obtain properly formed networks, assembling the DNA nanotubes is a crucial step. Errors during the synthesis process negatively impact the tube quality; therefore, it is recommended that HPLC or a more stringent process be used to purify the oligonucleotides. Since the formation of discrete rather than aggregated DNA nanotubes, as well as their length distribution, depends upon the equimolar stoichiometry of the n constituent oligonucleotides within the set, it is necessary to remeasure the concentrations of purchased strands, since given values can vary substantially from the actual concentration. This can be performed, for instance, by UV-Vis spectroscopy at an absorbance wavelength of 260 nm. We would like to note that molecular weights and extinction coefficients vary between the different sequences; therefore, the values to translate the absorbance into concentration should be determined for each DNA oligonucleotide. When using equipment optimized for small sample volumes, such as a NanoDrop, each measurement point should be taken several times and averaged. Comply with the linear range of detection of the spectrometer. Dilute the fraction used for concentration determination if necessary. Slight inaccuracies can have a large impact on the correct stoichiometry and quality of tube formation; therefore, the pipetting of the single strands must be as precise as possible. Subsequently, the final sample solution should be mixed thoroughly by slowly pipetting the sample up and down before placing it into the thermocycler. If strands have been modified with fluorescent dyes for visualization, all steps should be performed in an environment shielded from direct light, and the later addition of established anti-bleaching agents (*i.e.,* oxygen scavenging systems, such as glucose oxidase/catalase) is recommended. After the single strands have been mixed in the right buffer conditions, a temperature ramp is applied to hybridize the structures (**Figure 2A**). This temperature pattern follows the previously determined critical hybridization temperature, where the DNA double helices form. Several methods have been developed to analyze DNA hybridization kinetics (*i.e.,* native DNA UV absorbance[31], calorimetry[32], or fluorescent dyes[33]). In the latter method, dyes intercalate into DNA double helices, forming highly fluorescent complexes brighter than the unbound dyes. They partially bind to double-stranded but not to single-stranded DNA[34]. Therefore, such dyes have been applied to monitor DNA nanostructure self-assembly in the system[35] and can be used to identify ideal assembly conditions.

Initially, any double-stranded DNA within the sample, such as predefined and unpredicted duplexes, are denatured at a high temperature (90 °C) to avoid unintended base pairing. A subsequent gradual decrease in temperature (similar to **Figure 2A**) reduces the thermal motion of the DNA strands, enabling base paring events. Due to the minimization of the free energy, DNA strands preferentially hybridize at their complementary sequences. When a dsDNA-specific intercalating dye is applied, the brightness increases with the formation of highly fluorescent complexes, which is in turn a quantitative measure for newly formed double-stranded DNA[34]. The relative change of the fluorescence signal for the formation of 4HTs and 8HTs is plotted in **Figure 2B**. This relative change is calculated by averaging the fluorescence intensity for each temperature and subsequently subtracting the average value of the previous temperature. With decreasing temperature, an elevated fluorescence can be detected (**Figure 2B**), and the peak of this curve highlights the temperature where massive hybridization events occur. The drop of the curves refers to intensity values reaching a plateau. Depending on the DNA construct and its complexity (*e.g.,* a small or large set of DNA strands), the peak can be sharp (**Figure 2B**, blue curve) or broad (**Figure 2B**, green curve). When possible, this should be tested for every newly designed structure to ensure that the gradually decreasing portion of the temperature ramp contains the range where the formation of tubes via the formation of hybridized dsDNA segments is occurring. After the appropriate temperature regime is determined, nanostructures can be successfully assembled in very narrow temperature ranges (**Figure 2B**, blue curve), or even isothermally[35]. Note that the hybridization of multiple DNA strands in periodic lattices induces cooperative annealing effects[35,36], which support further DNA annealing. It should be considered that intercalating dyes do stretch DNA helices beyond their standard 10.5 base pairs per helical turn configuration, thus altering the overall geometry of the tubes. Therefore, it is not advisable to raise the dye concentration over one molecule per 900 DNA base pairs[35]. Furthermore, the peak assembly temperature may deviate from the actual optimal annealing temperature. To achieve high precision and to determine the best condition for tube formation, DNA hybridization should be investigated during many slowly changing temperature steps, which should be double-checked with agarose gel electrophoresis. For the case of the DNA nanotubes, we established a three-step protocol. First, the sample is heated

to 90 °C to denature the DNA into single strands. Subsequently, a broad temperature range (around the assembly peak of the fluorescence signal) is covered. In our case, a range of 10 °C is covered, ranging from 65 °C to 55 °C, with a step of -0.5 °C every 30 min. In the final step, the temperature should rapidly drop to room temperature - or, as in our case, 20 °C - to prevent any unfavorable interactions at intermediate temperatures (**Figure 2A**). Usually, thermocyclers heat the samples from colder temperatures. Therefore, it is important to adjust the temperature of the lid accordingly to limit the evaporation of liquid in the sample during assembly, which increases the final sample concentration.

If the *n*HTs are formed appropriately, they arrange into purely entangled networks (**Figure 3**), without interactions causing crosslinking effects between distinct tubes. Crosslinks would presumably result from unpaired DNA segments extending from defects along a tube or at sticky ends, which would be free to pair with complementary single-stranded segments on neighboring tubes. These effects would induce non-linear properties, such as strain hardening (increasing *G*' for larger strains), but they are absent in entangled networks (**Figure 4**). The displayed γ-sweeps also reveal the appropriate linear strain regimes for rheological measurements in general. Above a certain threshold, the network ruptures or loses contact with the plates of the rheometer, which irreversibly damages the system. Therefore, applied strains should be in the linear regime to obtain reliable data. Typically, a strain of 5% is sufficient to yield data well above the noise regime. Higher strains may be applied; however, they easily approach the rupture threshold, and results can be falsified due to measuring in the non-linear regime.

Rheological measurements require a careful, consistent preparation of the sample and carefully considered measurement protocols to obtain reproducible and interpretable results. The central point is to establish a completely random, isotropic network between the rheometer plates since these networks are mostly the only reproducible structure. Thus, rather long equilibration times (typically around 2 h, sometimes even more) are needed to disperse any ordering effects that occur due to shear-induced alignment during the pipetting of the sample. Pre-test experiments are recommended for recording the time evolution (time sweep) of the system during equilibration in order to determine the necessary time frame. Once the signals reach plateaus without further changes, the system is equilibrated. Once equilibration conditions have been determined, the desired tests, such as a strain ramp or f- or γ-sweeps, can be executed. Testing a broad spectrum of strains can ultimately destroy the network or the connection to the plates. However, if tests are limited to strains below the rupture threshold, strain ramps and sweeps can be iteratively repeated to investigate potential aging or hysteresis effects. In the case of *f*-sweeps, measurement times can vary substantially. Testing low frequencies dramatically prolongs the experiments, since one oscillation may take several minutes. Note that, in the case of *n*HTs, *f*-sweeps reveal that the elastic modulus *G*' exceeds the viscous modulus *G*'' by approximately one order of magnitude, which illustrates the predominant elastic response of these systems (**Figure 5**). Generally, the different types of experiments can be accompanied by short *f*-sweeps before and after the main experiment to verify that the system remained undisturbed by the measurement itself. However, some machines have to change the underlying motor mode for the different types of measurements, especially when changing from dynamic experiments (*e.g.,* oscillations for *f*-sweeps) to a static strain ramp. This change is often accompanied by spontaneous large strains destroying the network and tempering subsequent measurements. Thus, it is recommended to check the specifications of the rheometer used.

Rheology experiments on actin-based systems reveal a dramatic effect of protein denaturation occurring at the air-water interface of the system. Denatured proteins adhere unspecifically to each other, thereby forming a dense gel that can highly dominate the mechanical properties of the entire system. To prevent the direct contact of the sample with the surrounding air, passivation techniques that also suppress the evaporation of the water content of the sample can be used. Three potential methods are: (i) surrounding the sample chamber with the same buffer as in the sample; (ii) using surfactants to cover the interface due to their hydrophobic and hydrophilic domains (care must be taken, since some surfactants interfere with polymer conformations); or (iii) employing more biologically compatible lipids, with similar effects as surfactants. It should be noted that *n*HTs were not found to be subject to denaturation effects at the interface, and results are independent of the passivation method (**Figure 6**), which eliminates a major potential source of error. Generally, the sample chamber should always be sealed with a cap, which can be equipped with damp sponges to increase the humidity in the chamber, suppressing evaporation.

As briefly described previously, a potential error source in DNA-based systems is unhybridized DNA, such as unpaired single-stranded DNA overhangs at defects or at the ends of the nanotubes, which might cause additional crosslinking effects. To investigate and/or eliminate this possibility, complementary short strands can be used to cap these sticky ends. However, our own investigations showed that the addition of capping strands had no effect on the introduced *n*HTs, and the behavior of the entangled networks remained unchanged (**Figure 7**). However, capping sticky ends with complementary sequences can be useful for other DNA-based (and more complex) systems to suppress undesired interactions. Additionally, samples of *n*HTs should be pipetted carefully (*e.g.,* for dilution steps and sample preparation) to prevent any breaking or other damage to the tubes. If the solution is pipetted too roughly, the tubes break uncontrollably, exposing large numbers of sticky ends at defect points, leading to undesired interactions among the tubes and potential crosslinking in the system. This interferes with the signal and leads to stiffening effects, as well as to non-linear effects such as strain hardening, which becomes visible in γ-sweeps (**Figure 8**). Thus, pipetting the entangled solution should only be done slowly and using pipette tips with a rather large diameter (cutting the end of a pipette tip is advisable) to reduce the shear forces on the tubes.

In conclusion, DNA nHTs are a suitable and highly adaptable model system to study the semiflexible polymers and bulk networks formed from these filaments, representing a new class of mechanically tunable hydrogels. If the tubes are prepared carefully, they can be used to test the impact of the l_p of the filaments in various cases. The bulk rheological measurement of entangled networks, for instance, reveals that the theoretically predicted dependencies of the elastic modulus with concentration and l_p are inconsistent with the experimentally derived scaling laws (**Figure 9**)[9]. This study emphasizes that the elasticity of a network can be increased by increasing the stiffness of the underlying polymers. Traditionally, increasing the stiffness of a hydrogel was achieved either by adding more polymers to the solution or by inducing crosslinks (physical or chemical) between neighboring polymers[37,38]. However, a higher molecular content is also associated with a reduced mesh size, which can limit applications such as 3D cell culture. Crosslinks, on the other hand, can induce complex morphological changes within the underlying network architecture, which further complicates the precise tuning of mechanical properties[39]. Using networks of *n*HTs, however, allows for a complete decoupling of these parameters, whereby the stiffening effects can be induced by solely changing the stiffness of the underlying filaments while leaving the mesh size unchanged. Furthermore, the tube architectures can be specifically altered to selectively integrate additional effects such as crosslinking, which, similarly in entangled networks, creates further possibilities to experimentally test theoretical predictions for parameters such as l_p or crosslink size and strength for networks. In general, the programmable architecture broadens the scope of applications, allowing for the study of l_p-dependent effects not only in bulk, but also on the single-molecule level. Labeled tubes can be embedded in the network to study, for instance, the dependency of l_p on the one-dimensional motion of a filament in tube-like confinement, commonly referred to reptation (**Figure 10**)[9]. If this diffusive motion is visible, it also verifies the entangled nature of the network, since it would

be suppressed by crosslinking effects. Analyzing the underlying dynamics also reveals the mesh size of the network. Furthermore, these tubes can be used to investigate the dependency of the stiffness and chirality of the underlying tubes on the formation of bundles[40,41,42,43,44,45] or higher-order structures, such as star-like asters[46,47,48,49,50], which can be induced by crosslinking effects or via molecularly crowded environments[27].

Disclosures

The authors have nothing to disclose.

Acknowledgements

We acknowledge funding by DFG (1116/17-1) and the Leipzig School of Natural Sciences "BuildMoNa" (GSC 185). This work has been supported through the Fraunhofer Attract project 601 683. T. H. acknowledges funding from the European Social Fund (ESF-100077106).

References

1. Huber, F. *et al.* Emergent complexity of the cytoskeleton: from single filaments to tissue. *Adv Phys.* **62** (1), 1-112 (2013).
2. Kratky, O., Porod, G. Röntgenuntersuchung gelöster Fadenmoleküle. *Recl Trav Chim Pays-Bas.* **68** (12), 1106-1122 (1949).
3. Saitô, N., Takahashi, K., Yunoki, Y. The Statistical Mechanical Theory of Stiff Chains. *J Phys Soc Jpn.* **22** (1), 219-226 (1967).
4. Doi, M., Edwards, S. F. *The Theory of Polymer Dynamics.* 73. Oxford University Press. Oxford, UK. (1986).
5. Mueller, O., Gaub, H. E., Baermann, M., Sackmann, E. Viscoelastic moduli of sterically and chemically cross-linked actin networks in the dilute to semidilute regime: measurements by oscillating disk rheometer. *Macromolecules.* **24** (11), 3111-3120 (1991).
6. MacKintosh, F. C., Käs, J., Janmey, P. A. Elasticity of Semiflexible Biopolymer Networks. *Phys Rev Lett.* **75** (24), 4425-4428 (1995).
7. Gardel, M. L. Elastic Behavior of Cross-Linked and Bundled Actin Networks. *Science.* **304** (5675), 1301-1305 (2004).
8. Sonn-Segev, A., Bernheim-Groswasser, A., Diamant, H., Roichman, Y. Viscoelastic Response of a Complex Fluid at Intermediate Distances. *Phys Rev Lett.* **112** (8) (2014).
9. Schuldt, C. *et al.* Tuning Synthetic Semiflexible Networks by Bending Stiffness. *Phys Rev Lett.* **117** (19) (2016).
10. Käs, J. et al. F-actin, a model polymer for semiflexible chains in dilute, semidilute, and liquid crystalline solutions. *Biophys J.* **70** (2), 609-625 (1996).
11. Ross-Murphy, S. B. Structure-property relationships in food biopolymer gels and solutions. *J Rheol.* **39** (6), 1451-1463 (1995).
12. Fletcher, D. A., Mullins, R. D. Cell mechanics and the cytoskeleton. *Nature.* **463** (7280), 485-492 (2010).
13. Hinner, B., Tempel, M., Sackmann, E., Kroy, K., Frey, E. Entanglement, Elasticity, and Viscous Relaxation of Actin Solutions. *Phys Rev Lett.* **81** (12), 2614-2617 (1998).
14. Palmer, A., Mason, T. G., Xu, J., Kuo, S. C., Wirtz, D. Diffusing Wave Spectroscopy Microrheology of Actin Filament Networks. *Biophys J.* **76** (2), 1063-1071 (1999).
15. Gardel, M. L., Valentine, M. T., Crocker, J. C., Bausch, A. R., Weitz, D. A. Microrheology of Entangled F-Actin Solutions. *Phys Rev Lett.* **91** (15) (2003).
16. Liu, J. *et al.* Microrheology Probes Length Scale Dependent Rheology. *Phys Rev Lett.* **96** (11) (2006).
17. Golde, T., Schuldt, C., Schnauß, J., Strehle, D., Glaser, M., Käs, J. Fluorescent beads disintegrate actin networks. *Phys Rev E.* **88** (4) (2013).
18. Isambert, H., Maggs, A. C. Dynamics and Rheology of Actin Solutions. *Macromolecules.* **29** (3), 1036-1040 (1996).
19. Käs, J., Strey, H., Sackmann, E. Direct imaging of reptation for semiflexible actin filaments. *Nature.* **368** (6468), 226-229 (1994).
20. Schmidt, C. F., Baermann, M., Isenberg, G., Sackmann, E. Chain dynamics, mesh size, and diffusive transport in networks of polymerized actin: a quasielastic light scattering and microfluorescence study. *Macromolecules.* **22** (9), 3638-3649 (1989).
21. Kroy, K., Frey, E. Force-Extension Relation and Plateau Modulus for Wormlike Chains. *Phys Rev Lett.* **77** (2), 306-309 (1996).
22. Morse, D. C. Tube diameter in tightly entangled solutions of semiflexible polymers. *Phys Rev E.* **63** (3) (2001).
23. Broedersz, C. P., MacKintosh, F. C. Modeling semiflexible polymer networks. *Rev Mod Phys.* **86** (3), 995-1036 (2014).
24. Tassieri, M., Evans, R. M. L., Barbu-Tudoran, L., Khaname, G. N., Trinick, J., Waigh, T. A. Dynamics of Semiflexible Polymer Solutions in the Highly Entangled Regime. *Phys Rev Lett.* **101** (19) (2008).
25. Hinsch, H., Frey, E. Non-Affine Shear Modulus in Entangled Networks of Semiflexible Polymers. *arXiv:0907.1875[cond-mat].* (2009).
26. Yin, P. *et al.* Programming DNA Tube Circumferences. *Science.* **321** (5890), 824-826 (2008).
27. Glaser, M. *et al.* Self-assembly of hierarchically ordered structures in DNA nanotube systems. *New J Phys.* **18** (5), 055001 (2016).
28. Schiffels, D., Liedl, T., Fygenson, D. K. Nanoscale Structure and Microscale Stiffness of DNA Nanotubes. *ACS Nano.* **7** (8), 6700-6710 (2013).
29. Hariadi, R. F., Yurke, B., Winfree, E. Thermodynamics and kinetics of DNA nanotube polymerization from single-filament measurements. *Chem Sci.* **6** (4), 2252-2267 (2015).
30. de Gennes, P. G. Reptation of a Polymer Chain in the Presence of Fixed Obstacles. *J Chem Phys.* **55** (2), 572-579 (1971).
31. Huss, V. A. R., Festl, H., Schleifer, K. H. Studies on the spectrophotometric determination of DNA hybridization from renaturation rates. *Syst Appl Microbio.* **4** (2), 184-192 (1983).
32. Breslauer, K. J., Frank, R., Blöcker, H., Marky, L. A. Predicting DNA duplex stability from the base sequence. *Proc Natl Acad Sci U S A.* **83** (11), 3746-3750 (1986).
33. You, Y., Tataurov, A. V., Owczarzy, R. Measuring thermodynamic details of DNA hybridization using fluorescence. *Biopolymers.* **95** (7), 472-486 (2011).
34. Zipper, H. Investigations on DNA intercalation and surface binding by SYBR Green I, its structure determination and methodological implications. *Nucleic Acids Res.* **32** (12), e103-e103 (2004).
35. Sobczak, J.-P. J., Martin, T. G., Gerling, T., Dietz, H. Rapid Folding of DNA into Nanoscale Shapes at Constant Temperature. *Science.* **338** (6113), 1458-1461 (2012).

36. Snodin, B. E. K., Romano, F., Rovigatti, L., Ouldridge, T. E., Louis, A. A., Doye, J. P. K. Direct Simulation of the Self-Assembly of a Small DNA Origami. *ACS Nano.* **10** (2), 1724-1737 (2016).
37. Das, R. K., Gocheva, V., Hammink, R., Zouani, O. F., Rowan, A. E. Stress-stiffening-mediated stem-cell commitment switch in soft responsive hydrogels. *Nat Mater.* **15** (3), 318-325 (2015).
38. Sharma, A. *et al.* Strain-controlled criticality governs the nonlinear mechanics of fibre networks. *Nat Phys.* **12** (6), 584-587 (2016).
39. Lieleg, O., Claessens, M. M. A. E., Bausch, A. R. Structure and dynamics of cross-linked actin networks. *Soft Matter.* **6** (2), 218-225 (2010).
40. Claessens, M. M. A. E., Semmrich, C., Ramos, L., Bausch, A. R. Helical twist controls the thickness of F-actin bundles. *Proc Natl Acad Sci U S A.* **105** (26), 8819-8822 (2008).
41. Claessens, M. M. A. E., Bathe, M., Frey, E., & Bausch, A. R. Actin-binding proteins sensitively mediate F-actin bundle stiffness. *Nat Mater.* **5** (9), 748-753 (2006).
42. Schnauß, J., Händler, T., & Käs, J. Semiflexible Biopolymers in Bundled Arrangements. *Polymers.* **8** (8), 274 (2016).
43. Heussinger, C., Schüller, F., Frey, E. Statics and dynamics of the wormlike bundle model. *Phys Rev E.* **81** (2) (2010).
44. Schnauß, J. *et al.* Transition from a Linear to a Harmonic Potential in Collective Dynamics of a Multifilament Actin Bundle. *Phys Rev Lett.* **116** (10) (2016).
45. Strehle, D. *et al.* Transiently crosslinked F-actin bundles. *Eur Biophys J.* **40** (1), 93-101 (2011).
46. Backouche, F., Haviv, L., Groswasser, D., Bernheim-Groswasser, A. Active gels: dynamics of patterning and self-organization. *Phys Biol.* **3** (4), 264-273 (2006).
47. Surrey, T. Physical Properties Determining Self-Organization of Motors and Microtubules. *Science.* **292** (5519), 1167-1171 (2001).
48. Nedelec, F. J., Surrey, T., Maggs, A. C., Leibler, S. Self-organization of microtubules and motors. *Nature.* **389** (6648), 305-308 (1997).
49. Smith, D. *et al.* Molecular Motor-Induced Instabilities and Cross Linkers Determine Biopolymer Organization. *Biophys J.* **93** (12), 4445-4452 (2007).
50. Huber, F., Strehle, D., Schnauß, J., Käs, J. Formation of regularly spaced networks as a general feature of actin bundle condensation by entropic forces. *New J Phys.* **17** (4), 043029 (2015).

